Catal Lett (2007) 119:29–39
DOI 10.1007/s10562-007-9148-z

Hydrogen Production by Steam Reforming of Ethanol on Potassium-Doped $12CaO \cdot 7Al_2O_3$ Catalyst

Ting Dong · Zhaoxiang Wang · Lixia Yuan · Youshifumi Torimoto · Masayoshi Sadakata · Quanxin Li

Received: 15 May 2007 / Accepted: 3 June 2007 / Published online: 23 June 2007

Abstract The performance of hydrogen production from steam reforming of ethanol were investigated by using the K-doped $12CaO \cdot 7Al_2O_3$ catalyst (defined as C12A7–O^-/*x*%K). The conversion of ethanol and hydrogen yield over C12A7–O^-/*x*%K catalyst mainly depended on the temperature, K-doping amount, steam-to-carbon ratios (S/C) and contact time (W/F). In order to identify the catalyst's characteristic and active species on the catalyst's surface, Brunauer-Emmett-Teller (BET) surface area, CO_2 temperature programmed desorption (CO_2TPD), X-ray diffraction (XRD), Fourier transform infrared (FT–IR) and X-ray photoelectron spectroscopy (XPS) were carried out. Based on the characterization, it was found that active oxygen species and doped potassium play important roles in steam reforming of ethanol over C12A7–O^-/27.3%K catalyst.

Keywords Hydrogen production · Ethanol · Steam reforming

1 Introduction

Hydrogen is the ideal source of chemical energy that can be converted to electricity directly and efficiently via fuel cells with zero emissions of hazardous species such as volatile organic compounds, nitrogen oxides and carbon oxides [1, 2]. A hydrogen production unit combined with a fuel cell power generator is a promising alternative for immobile and mobile applications in the future. Currently, almost 90% of the H_2 in the merchant market is derived from the steam reforming of natural gas or the light oil fraction at high temperature [3]. However, hydrogen production from natural gas is always associated with the emission of greenhouse gases and local pollutants. On the other hand, H_2 production from ethanol steam reforming would not only be environmentally friendly, but also would open a new prospect for the utilization of the renewable resources that are globally available. Among different technologies proposed, attention was focused on the development of active, stable and selective catalyst for ethanol steam reforming reaction. At the moment, metal sintering and coke formation seems to represent the main problems to overcome. Supported transition metal catalysts, especially Co, Pt, Pd, Rh, Ru and Ni, were widely investigated [4–10]. Co-based catalysts even though have been proposed as appropriate systems for steam reforming of ethanol [4] could be affected by deactivation mainly by sintering and surface Co oxidation [5]. Among noble metal based catalysts, Rh is significantly more active and selective compared to Pt, Pd and Ru catalysts of similar metal loading [6–9]. Steam reforming of ethanol on Ni catalysts supported on La_2O_3, Al_2O_3, YSZ and MgO was also investigated [10]. The observed higher activity and stability of Ni/La_2O_3 was attributed to the formation of lanthanum oxycarbonate species ($La_2O_2CO_3$) which reacting with surface carbon deposited during reaction prevents the Ni deactivation. Ni–Cu bimetallic catalyst, recently proposed, looks interesting but coke formation drastically affects such systems [11]. Cu–Ni–K/γ-Al_2O_3

T. Dong · Z. Wang · L. Yuan · Q. Li (✉)
Department of Chemical Physics, Lab of Biomass Clean Energy, University of Science & Technology of China, Hefei, Anhui 230026, P.R. China
e-mail: liqx@ustc.edu.cn

Y. Torimoto · M. Sadakata
Department of Chemical System Engineering, School of Engineering, The University of Tokyo, 7-3-1 Hongo, Bunkyo-ku, Tokyo 113-8656, Japan

catalysts were proposed for ethanol gasification at low temperature: limitation due to diffusion resistance has been observed [12].

The microporous crystal $12CaO \cdot 7Al_2O_3$ (C12A7) has a cubic structure with a lattice constant of 1.1989 nm, which is characterized by a positive charged lattice framework $[Ca_{24}Al_{28}O_{64}]^{4+}$ including 12 subnanometer sized cages [13–17]. The two remaining O^{2-} ions are clathrated in the cages. The storage features of O^- anions in the bulk of C12A7 was first explored by Hosono et al. [13] and further clarified by Hayashi et al. [18]. Recently, we have found that the O^- anions stored in the cages of C12A7–O^- could be desorbed into the gas-phase by applying an extraction field under suitable temperature [19, 20]. We also observed that O^{2-} was able to substituted by other mono-charge anion X^- ($X^- = OH^-$, H^- etc.) to form the derivatives $[Ca_{24}Al_{28}O_{64}]^{4+} \cdot 4(X^-)$ (C12A7–X^-) [21–23]. It is well known that active O^- anion is a key intermediate in the anion chemistry [24–30], particularly in low-temperature oxidation of hydrocarbons [27–29]. Because C12A7–O^- has unique O^- storage and emission feature, this material can be used as a good catalyst to oxygenate or decompose some chemicals (e.g., hydrocarbons etc.). For example, C12A7 has been used as a catalyst mainly in the pyrolysis of n-hexane [31], n-heptane [32–34], methylcyclohexane [35] and partial oxidation of methane [36, 37]. More recently, we found the C12A7–O^- catalyst was active in hydroxylation of benzene [38] and steam reforming of bio-oil [39].

It is well known that compounds of alkali and alkaline earth metals are active catalysts for the gasification of carbon [40, 41]. Carbonates and hydroxides of these metals have better catalytic activity than the other salts [42]. Although a limitation of the C12A7 catalyst is the coke deposition on the catalyst, K_2CO_3 is known to be an active catalyst for the steam-coke reaction, and many studies found that the coke deposition on the catalyst was significantly decreased when C12A7 was impregnated with K_2CO_3 [43] or appropriate promoters [44] to enhance the coke-steam reaction. On the other hand, due to the high reaction temperature (~973 K), K_2CO_3, which has the highest melting point compared to the other alkali carbonates, was chosen as the gasifying agent.

In the present study steam reforming reaction of ethanol over the K-doped catalyst of C12A7–O^-/*x*%K have been studied. The dependence of the catalytic activity and selectivity on the content of potassium, reaction temperature, steam-to-carbon ratios (S/C) and contact time were investigated. Long-term experiment and catalyst characterization were also performed.

2 Experimental

2.1 Catalyst Preparation

The C12A7–O^- sample was prepared by a solid-state reaction at 1623 K for 16 h. The more detailed process for preparation can be found elsewhere [22, 23, 38, 39]. The C12A7–O^- pellet was powdered and mechanically mixed with various content of K_2CO_3. Finally, these mixtures were calcined in air by a muffle furnace at 773 K for 4 h. The potassium loading was 3.9, 11.7, 19.5, 27.3, 35.1 wt.% of catalyst, which was measured by inductively coupled plasma atomic emission spectroscopy (ICP-AES). These series materials were defined as C12A7–O^-/*x*%K (*x* = 3.9, 11.7, 19.5, 27.3, 35.1). Finally, all the sintered materials were crushed into granules (250–350 μm).

Nickel catalysts supported on γ–Al_2O_3 was prepared by the wet impregnation method using nickel nitrate as the metal precursor. A known amount of $Ni(NO_3)_2$ was dissolved in water and γ–Al_2O_3 was added to the solution under continuous stirring. The slurry was dried at 383K for 24 h and then calcined in air at 773 K for 4 h for complete decomposition of nickel nitrate. The nickel loading was 10 wt.%. Before steam reforming reaction, the catalyst sample was reduced at 773 K in H_2 flow for 5 h.

Rhodium catalysts were prepared by impregnation of the support γ–Al_2O_3 with an aqueous solution of the metal precursor salt $Rh(NO_2)_3$. The slurry was dried at 383 K for 24 and then calcined in air at 973 K for 4 h for complete decomposition of rhodium nitrate. The rhodium loading of the catalyst was 1 wt.%. Before reaction, the catalyst sample was reduced at 773 K in H_2 flow for 5 h.

2.2 Measurements of Activity and Selectivity

Catalytic performance tests have been conducted in the temperature range of 723–973 K over the prepared catalysts with 250–350 μ m particles size. In a typical experiment a desired flux of argon passed through the water–ethanol mixture contained in a saturator, and then directed to the flow reactor, which contained 0.3 g of the catalyst diluted with an equal amount and size of quartz particles. The temperature value in the catalyst bed was continuously monitored and measured. The flow rate of the gas was controlled by mass flowmeter. The gas hourly space velocity (GHSV) was defined as the gas flow rate mL h^{-1}) to the catalyst volume (mL) ratio. The contact time, described by W/F, is defined as the ratio of the mass of catalyst (g) to the molar flow rate of the inlet ethanol (mol h^{-1}). The reactants and products were analyzed by an on-line gas chromatograph, using Molecular Sieve 5A and Porapak Q columns and a thermal conductivity detector.

2.3 Catalyst Characterization

The Brunauer–Emmett–Teller (BET) surface areas of the catalysts were determined using a COULTER SA 3100 analyzer with nitrogen as the sorbate at 77 K.

The basic property of the catalyst were characterized using the temperature programmed desorption of CO_2(CO_2TPD). The experiments were performed using a quartz-made microreactor with 200 mg catalyst. The catalysts were treated at 773 K for 5 h in an argon flow of 20 mL min^{-1} prior to the TPD measurement. The pretreated samples were saturated with CO_2 at room temperature for 30 min (20 mL min^{-1}). Then the samples were flushed with Ar flowing at 20 mL min^{-1} for 30 min, afterwards the temperature was increased to 1073 K at a heating rate of 10 K/min. Gas that desorbed was monitored using a mass spectrometer (Balzers, GSD 300 OmniStar).

Inductively coupled plasma atomic emission spectroscopy (ICP-AES) were employed to estimate the total doped metal content in the catalysts before and after the steam reforming experiments by using an Atomscan Advantage ICP-AES system (Thermo Jarrell Ash Co.).

X-ray diffraction (XRD) measurements were employed to investigate the structure of the catalysts before and after the steam reforming experiments. The catalysts are generally crushed into powder with the average diameter of 20–30 μm. Powder X-ray diffraction patterns were recorded on an X'pert Pro Philips diffractometer with a Cu–Kα source. The measurement conditions were in the 2θ range of 10–80°, step counting time of 5 s, and step size of 0.017° at 298 K.

Fourier transform infrared (FT–IR) spectra were measured at 298 K by a Bruker EQUINOX55 FT-IR spectrometer with KBr pellet method. The samples for FT–IR measurements were mixed at a weight ratio of sample: KBr = 100:3, then ground and pressed by a pressure of 400 atm to a pellet with a diameter of 1.0 cm and a thickness of 0.3 mm. The infrared absorption spectra were recorded and analyzed.

The X-ray photoelectron spectroscopy (XPS) measurements were performed on a VG ESCALAB MKII instrument, using Mg–Ka primary radiation (15 keV, 10 mA). The normalized XPS intensities, which are proportional to the effective concentrations of the corresponding elements in the surface layer, were determined as the integrated peak area divided by their corresponding sensitivity factor. The C(1s) peak was used as a calibration standard for determining the peaks' position and the elemental concentration. The present XPS and FT–IR measurements were performed before and after the catalytic reforming experiments (i.e., not in-situ characterization), which provided indirect evidence for the changes of the catalysts' characteristics.

2.4 Kinetic Parameters Formulae

Ethanol conversion denoted as X_{EtOH}, hydrogen yield denoted as Y_{H_2}, and products selectivity (carbon oxides, methane, ethane acetaldehyde) denoted as S_P, are calculated according to Eqs. 1–3:

$$X_{EtOH} = \frac{\text{moles EtOH}_{in} - \text{moles EtOH}_{out}}{\text{moles EtOH}_{in}} \times 100\%, \quad (1)$$

$$Y_{H_2} = \frac{\text{moles } H_2}{\text{moles EtOH}_{in}}, \quad (2)$$

$$S_P = \frac{\text{moles P}}{\chi(\text{moles EtOH}_{in} - \text{moles EtOH}_{out})} \times 100\%, \quad (3)$$

where P stands for products (i.e., carbon oxides, methane, ethylene and acetaldehyde), χ is the stoichiometry factor (6 for H_2, 2 for C_1 and 1 for C_2 compounds).

All of the data presented were given as the average value. Generally, the experiments were repeated for three times. The difference for each repeating, in general, ranged from 0% to 15%.

3 Results and Discussion

3.1 Effect of Potassium Content on Catalyst Activity

The prepared catalysts, C12A7–O^- and C12A7–O^-/*x*%K were tested for steam reforming of ethanol at a given molar steam-to-carbon ratio (S/C = 1.5, i.e. H_2O/EtOH = 3) and a total gas hourly space velocity (GHSV = 10,000 h^{-1}) at 973 K under atmospheric pressure. The results are presented in Table 1. It was found that both C12A7–O^- catalyst and K-doped C12A7–O^- catalysts showed high activity for steam reforming of ethanol. The conversion of ethanol was over 90% on all prepared catalysts at 973 K and S/C = 1.5. On the other hand, the addition of potassium to C12A7–O^- catalyst significantly promoted H_2 yield for steam reforming of ethanol. As the potassium concentration of 27.3% in C12A7–O^-/*x*%K was added, a maximum hydrogen yield of 3.73 mol $H_2 \cdot (\text{mol } C_2H_5OH)^{-1}$ was obtained. Further increasing K concentration over 27.3% resulted in the decrease of the hydrogen yield.

The ethanol conversion was essentially due to ethanol cracking, dehydration, dehydrogenation and catalytic steam reforming, with major production of H_2, CO, CO_2, CH_4, C_2H_4 and CH_3CHO. By using the pure C12A7–O^- catalyst, a relatively large amount of coke was deposited on the catalyst and the reactor wall. The amount of ethylene was much higher over the C12A7–O^- catalyst, suggesting that C12A7–O^- promoted the ethanol dehydration reaction to ethylene, followed by polymerization of ethylene to

Table 1 The results of ethanol steam reforming over various catalysts and non-catalytic blank test at atmospheric pressure with T = 973 K, GHSV= 10,000 h^{-1}, and S/C = 1.5

	Y_{H_2} [b] (mol mol^{-1})	X^{a}_{EtOH} (%)	Dry gas composition (%)					
			H_2	CO	CH_4	CO_2	C_2H_4	CH_3CHO
C12A7–O^-	0.92	91.2	42.5	5.1	14.5	11.1	16.4	10.3
C12A7–O^-/3.9%K	2.95	97.8	62.3	9.2	8.3	16.4	0.8	2.9
C12A7–O^-/11.7%K	3.07	98.4	62.4	9.1	8.7	17.2	0.9	1.6
C12A7–O^-/19.5%K	3.22	99.3	63.4	8.8	8.2	16.9	0.6	2.0
C12A7–O^-/27.3%K	3.73	100	65.5	8.1	7.1	18.5	0.4	0.3
C12A7–O^-/35.1%K	3.02	97.1	62.9	8.1	8.1	17.4	0.6	2.8
10%Ni/γ-Al_2O_3	4.35	100	68.5	14.1	2.6	14.8	0.0	0.0
1%Rh/γ–Al_2O_3	5.58	100	73.6	6.1	0.0	20.3	0.0	0.0
Non-catalytic blank	0.42	42.1	46.7	5.2	6.7	6.0	10.6	24.8

[a] X_{EtOH}: Ethanol conversion defined by Eq. 1

[b] Y_{H_2} Hydrogen yield defined by Eq. 2

form coke [43]. However, it was found that the addition of potassium plays stimulative role in the hydrogen generation from ethanol steam reforming, which includes: (1) increasing the hydrogen yield, (2) decreasing the ethylene and acetaldehyde concentration in the product gas, and (3) significantly decreasing the coke deposited on the catalysts. Particularly, the C12A7–O^-/27.3%K catalyst showed a very promising performance. As compared with other C12A7–O^-/*x*%K (*x* = 3.9, 11.7, 19.5, 35.1) catalysts, not only the amount of ethylene and acetaldehyde, but also the amount of methane obviously decreased over C12A7–O^-/27.3%K. In present work, we mainly focused on the ethanol steam reforming reaction over C12A7–O^-/27.3%K catalyst. Table 1 also gives the ethanol steam reforming reaction data of 10%Ni/γ–Al_2O_3, 1%Rh/γ–Al_2O_3 catalyst and non-catalytic blank test at the same reaction conditions with that of C12A7–O^-/*x*%K. It was observed that rhodium catalyst gave the highest H_2 yield of 5.58 mol H_2 · (mol $C_2H_5OH)^{-1}$ of all catalysts tested and the C12A7–O^- / 27.3%K gave a H_2 yield of 3.73 mol H_2 · (mol $C_2H_5OH)^{-1}$, which was closed to that of nickel catalyst. Compared with rhodium catalyst, the C12A7–O^-/*x*%K catalyst is cheaper and more environmentally friendly. Non-catalytic blank test gave the much lower H_2 yield of 0.42 mol H_2 · (mol $C_2H_5OH)^{-1}$ and lower ethanol conversion of 42.1% than those as catalysts were used. Figure 1 presents the H_2 yield and the ethanol conversion of non-catalytic blank test and over C12A7–O^-/27.3%K catalyst as a function of reaction temperature. With temperature increasing from 773 K to 973 K, for non-catalytic blank test, H_2 yield increased from 0.04 to 0.42 mol H_2 · (mol $C_2H_5OH)^{-1}$, ethanol conversion increased smoothly from 10.7% to 42.1%. While over C12A7–O^-/27.3%K catalyst, H_2 yield increased from 0.16 to 3.73 mol H_2· (mol $C_2H_5OH)^{-1}$, ethanol conversion increased rapidly from 15.2% to 100%. Thus, the catalytic steam reforming reaction over C12A7–O^-/27.3%K catalyst plays an important role to the hydrogen yield. The material balance was performed over a period of 4 h. Table 2 presents the overall material balance of the ethanol steam reforming reaction. For all the experiments performed, the overall material balance closures, defined as outlet mass/inlet mass (wt.%), was 100 ± 9%.

3.2 Effect of Reaction Temperature

Ethanol steam reforming reaction was investigated over C12A7–O^-/27.3%K catalyst at a given molar steam-to-carbon ratio (S/C = 1.5) and a total gas hourly space velocity (GHSV = 10,000 h^{-1}) under temperature ranging from 723 K to 973 K. In Fig. 2a and b, the yield of H_2, the conversion of ethanol and selectivity of other detectable

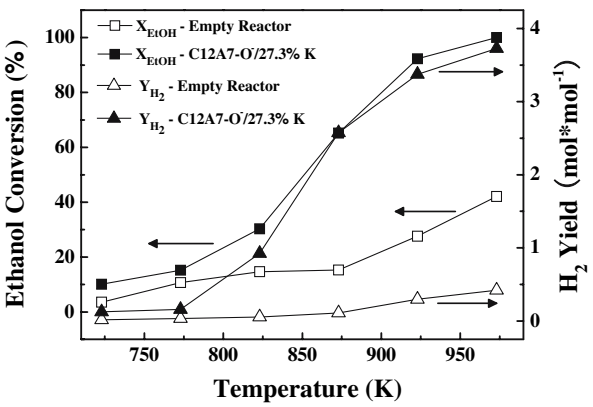

Fig. 1 Effect of reaction temperature on the H_2 yield and the ethanol conversion of non-catalytic test (open symbols) and C12A7–O^-/27.3%K catalyst (filled symbols) at S/C = 1.5, GHSV = 10,000 h^{-1}, and P = 1 atm

Table 2 Overall material balance for ethanol steam reforming. T = 973 K, GHSV = 10,000 h^{-1}, and S/C = 1.5

Catalyst	Outlet mass/Inlet mass (wt.%)									
	H_2	CO	CH_4	CO_2	C_2H_4	CH_3CHO	Coke	C_2H_5OH	H_2O	Total
C12A7–O^-	1.8	3.0	4.9	10.3	9.6	9.5	2.8	4.0	45.3	91.2
C12A7–O^-/3.9%K	5.9	12.2	6.3	34.0	0.9	6.0	1.1	1.0	36.2	103.6
C12A7–O^-/11.7%K	6.1	12.5	6.8	37.1	1.2	3.4	0.2	0.7	27.1	95.1
C12A7–O^-/19.5%K	6.4	12.5	6.6	37.6	0.8	4.4	a	0.3	31.0	99.6
C12A7–O^-/27.3%K	8.1	13.7	6.7	48.0	0.8	0.9	a	0	27.3	105.5
C12A7–O^-/35.1%K	6.0	10.9	6.2	36.8	0.8	5.9	a	1.3	28.9	96.8
10%Ni/γ–Al_2O_3	8.8	25.3	2.7	41.8	0	0	0.5	0	23.6	102.7
1%Rh/γ–Al_2O_3	11.2	12.9	0	67.6	0	0	a	0	9.2	100.9
Non-catalytic blank	0.9	1.3	1.0	2.4	2.7	9.9	4.2	26.6	43.2	92.2

a, Not found

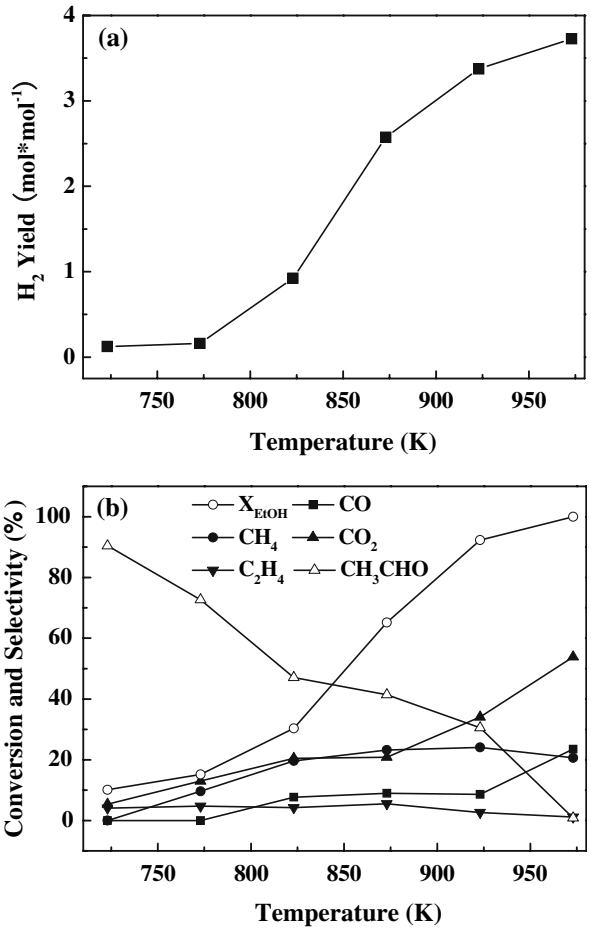

Fig. 2 Effect of reaction temperature on the (**a**) H_2 yield and (**b**) ethanol conversion, selectivity of CO_2, CO, CH_4, C_2H_4, CH_3CHO, obtained over C12A7–O^-/27.3%K catalyst at S/C = 1.5, GHSV = 10,000 h^{-1}, and P = 1 atm

products (CO, CH_4, CO_2, C_2H_4, CH_3CHO) from steam reforming of ethanol are depicted as a function of reaction temperature. As temperature lower than 723 K, H_2 yield was not detected due to low ethanol conversion. With further increasing temperature, both the ethanol conversion and H_2 yield significantly increased. Ethanol conversion was 100% and H_2 yield reached a maximum value of 3.73 mol $H_2 \cdot (\text{mol } C_2H_5OH)^{-1}$ at 973 K in our investigated temperature range.

As the reaction temperature increased, H_2 yield was mainly controlled by ethanol dehydrogenation reaction (reaction 4), ethanol cracking to methane (reaction 5) followed by steam reforming of CH_4 (reaction 6), ethanol steam reforming to syngas (CO + H_2) (reaction (7)) and the water-gas shift reaction (reaction (8)) [45]:

$$C_2H_5OH \rightarrow CH_3CHO + H_2, \quad (4)$$

$$C_2H_5OH \rightarrow CH_4 + CO + H_2, \quad (5)$$

$$CH_4 + H_2O \rightarrow CO + 3H_2, \quad (6)$$

$$C_2H_5OH + H_2O \rightarrow 2CO + 4H_2, \quad (7)$$

$$CO + H_2O \rightarrow CO_2 + H_2. \quad (8)$$

On the other hand, observed from Fig. 2b, at the lower temperature, the main by-product in the steam reforming reaction of ethanol was acetaldehyde, which was produced through ethanol dehydrogenation reaction (reaction 4). When increased temperature from 723 K to 973 K, selectivity of acetaldehyde remarkably decreased from 90.5% to 0.9%, indicating that the acetaldehyde cracking and catalytic steam reforming of acetaldehyde occur at a higher temperature. The selectivity of methane gradually increased from 0% to 19.6% in the range 723–830 K, and remained a constant with about 20% over 830 K. The methane is produced by cracking of acetaldehyde [45]:

$$CH_3CHO \rightarrow CH_4 + CO. \quad (9)$$

With increasing temperature, acetaldehyde largely cracked, and both the selectivity of CH_4 and CO increased due to the reaction 9. Furthermore, as reaction temperature increased, the rate of steam reforming reactions of methane and acetaldehyde as well as the rate of water-gas shift reaction increased, leading to a simultaneous increase in the concentration of CO_2 and H_2. It was also found that carbon deposition was negligible under the molar ratio of water to ethanol being equal and higher than the stoichiometry (i.e. S/C = 1.5).

3.3 Effect of Steam to Carbon Ratio

Besides temperature, S/C ratio is another important factor to influence the steam reforming process of ethanol. Fig. 3a and b show the H_2 yield and the ethanol conversion over C12A7–O^-/27.3%K catalyst, measured as a function of temperature at three different steam-to-carbon ratios (S/C=1.5, 4.0, 12.0). With increasing S/C ratio, both the conversion of ethanol and H_2 yield increase. This indicates that the increase of water content significantly promotes the steam reforming reaction of ethanol. As the S/C ratio was 12.0 at the temperature of 973K, the H_2 yield highly reached 4.73 mol · mol^{-1}.

Figure 4 presents the influence of S/C ratio on the selectivity of all products obtained over C12A7–O^-/27.3%K catalyst at a given temperature of 973 K, GHSV = 10,000 h^{-1} and P = 1 atm. With increasing S/C ratio from 1.5 to 4.0, H_2 selectivity increases from 62.1% to 76.1%, CO_2 selectivity increases from 53.8% to 67.1%, while CO selectivity decreases from 23.5% to 9.8% and selectivity to CH_3CHO decreases from 0.9% to zero. As further increasing S/C from 4.0 to 12.0, no distinct influence on the selectivity of H_2, CO, CO_2 and CH_3CHO was observed. Also, no prominent change was observed to the selectivity of CH_4 and C_2H_4. Moreover, the most significant effect upon increasing S/C ratio is to increase the H_2/CO and CO_2/CO ratio, as it was shown in Fig. 5. This performance is attributed to the water gas shift reaction (reaction 8), as it strongly moves towards the CO_2formation with the consequent increase of H_2 and the decrease of the CO concentration in the outlet stream.

3.4 Effects of Contact Time and Time on Stream

The effect of contact time (W/F) on the performance of the C12A7–O^-/27.3%K at S/C = 1.5 with the reaction temperature ranging from 723 K to 973 K is illustrated in Fig. 6a and b, respectively, where the yield of hydrogen and the conversion of ethanol with different contact time were plotted as function of temperature. As one can observe, both the H_2 yield and ethanol conversion increased with the increasing contact time (W/F) from

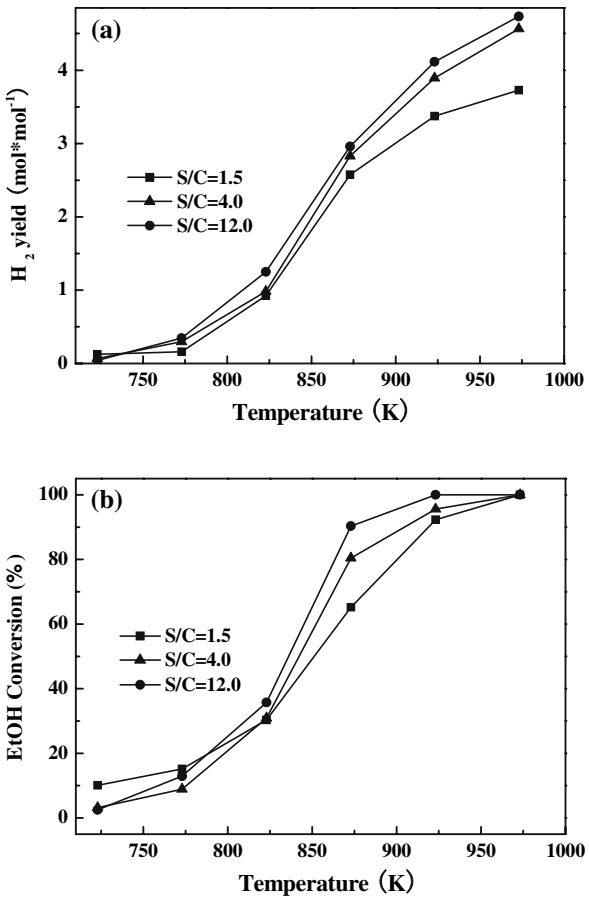

Fig. 3 Effect of reaction temperature on the (**a**) H_2 yield and (**b**) ethanol conversion at different S/C ratios (S/C = 1.5, 4, 12), obtained over C12A7–O^-/27.3%K catalyst at GHSV = 10,000 h^{-1}, and P = 1 atm

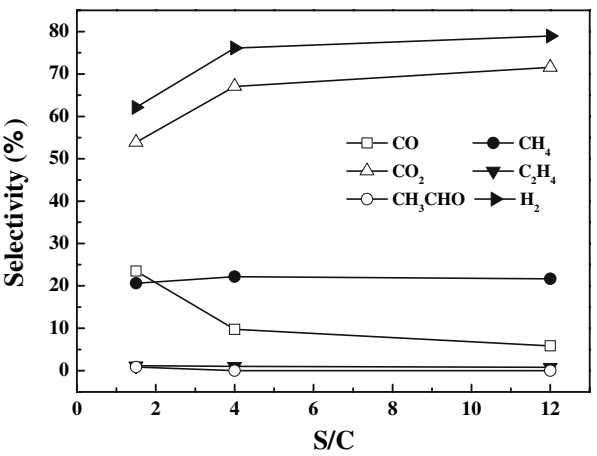

Fig. 4 Effect of S/C ratio on the selectivity of the products obtained over C12A7–O^- /27.3%K catalyst. The steam reforming condition: T = 973 K, GHSV = 10,000 h^{-1}, P = 1 atm

3.3 g·hr·mol^{-1} to 9.8 g·hr·mol^{-1}. This indicates that contact time is also an important factor for the steam reforming reaction of ethanol, and increasing the contact

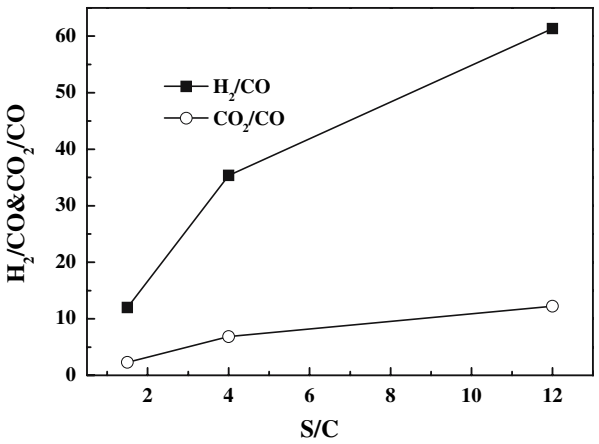

Fig. 5 Effect of the S/C ratio on the H_2 to the CO molar ratio (H_2/CO) and on the molar ratio of CO_2 to CO (CO_2/CO) obtained over C12A7–O^-/27.3%K catalyst. The steam reforming condition: T = 973 K, GHSV = 10,000 h^{-1}, P = 1 atm

time between the reactants and catalyst is in favor of steam reforming of ethanol.

The effect of time on stream on the H_2 yield, ethanol conversion and selectivity of the carbon-containing products at T = 973K, S/C = 1.5 and GHSV = 10,000h^{-1} over C12A7–O^-/27.3%K are depicted in Fig. 7a and b. It was found that H_2 yield, ethanol conversion and selectivity to the carbon-containing products were stable in our detected time range (about 700 min). Almost no carbon deposition was observed on the surface of the catalyst for 700 min. It is considered that the composition of potassium in the C12A7–O^-/27.3%K catalyst contributes to a significant decrease in the coke deposited on the catalyst due to the rate increase of the coke-steam reactions [43]. Present results show that C12A7–O^-/27.3%K is a stable catalyst and have a longer lifetime than conventional catalysts.

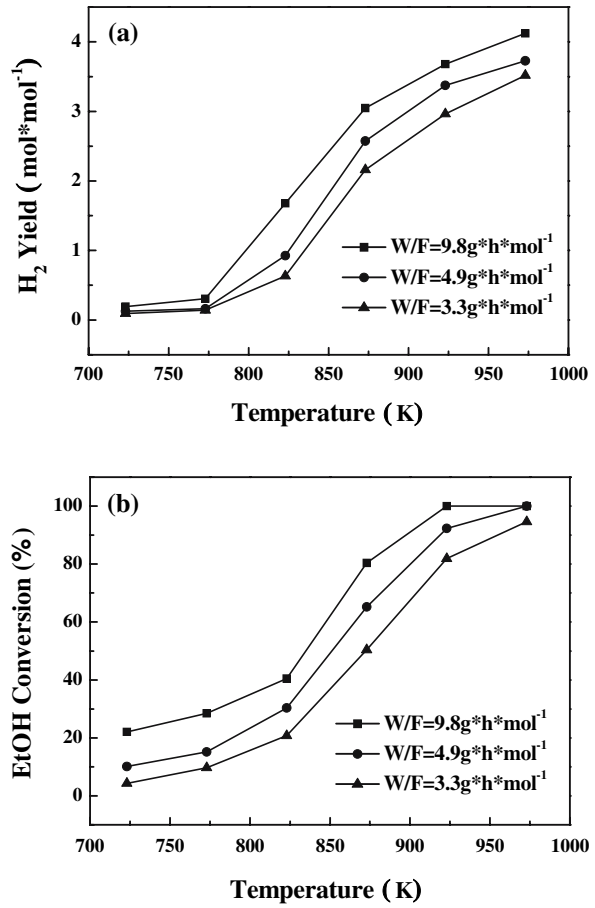

Fig. 6 Effect of reaction temperature on the (**a**) H_2 yield and (**b**) ethanol conversion at different contact time (W/F = 3.3, 4.9, 9.8 g h mol^{-1}) over C12A7–O^-/27.3%K catalyst. The steam reforming condition: S/C = 1.5, P = 1 atm

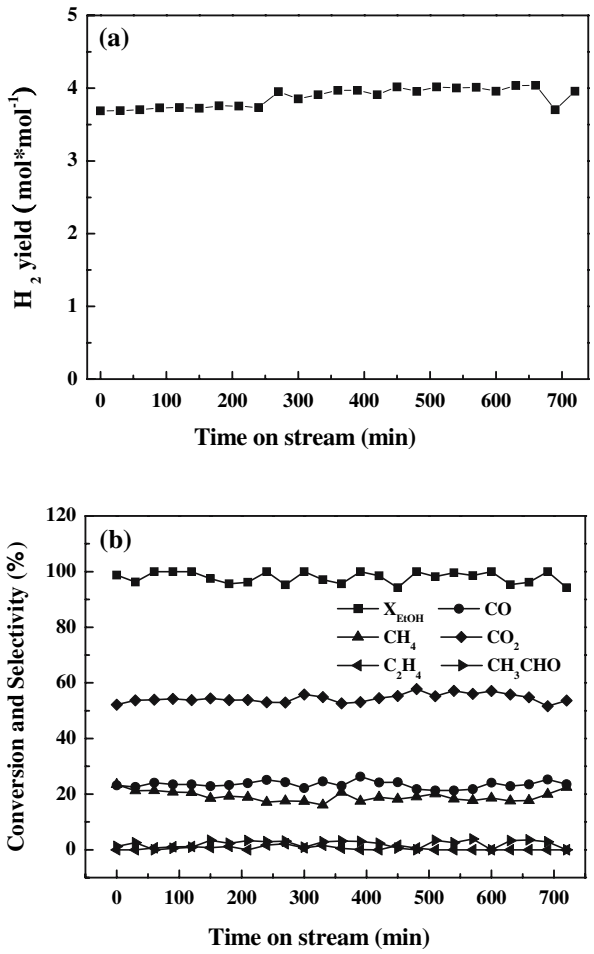

Fig. 7 Dependence of the (**a**) H_2 yield and (**b**) ethanol conversion and hydrocarbon selectivity on time on stream over C12A7–O^-/27.3%K catalyst. The steam reforming conditions: GHSV = 10,000 h^{-1}, T = 973 K, S/C = 1.5, P = 1 atm

3.5 Catalyst Characterization

The BET surface areas of the C12A7–O^- and C12A7–O^-/27.3%K catalysts were determined using a COULTER SA 3100 analyzer with nitrogen as the sorbate at 77 K. The BET surface area of C12A7–O^- catalyst is about 1.45 $m^2 \cdot g^{-1}$, and C12A7–O^-/27.3%K catalyst is about 1.94 $m^2 \cdot g^{-1}$. The amount of CO_2 desorbed from C12A7–O^- and C12A7–O^-/27.3%K was determined by the CO_2 TPD measurements. The C12A7–O^- catalyst had a site density of CO_2 adsorption sites of 1.85×10^{13} molecules cm^{-2}. As the potassium concentration of 27.3 wt% in C12A7–O^-/*x*%K was added, C12A7–O^-/27.3%K had a higher density of CO_2 adsorption sites of 4.85×10^{14} molecules cm^{-2}. It is well known that dehydrogenation of alcohols is a base–catalyst reaction, which is an important step (reaction 4) in the ethanol steam reforming reaction. Addition potassium to the C12A7–O^-/*x*%K, the amount of basic sites increased, leading to a better activity of the ethanol catalytic reforming reaction.

Three different samples (i.e. C12A7–O^-, fresh C12A7–O^-/27.3%K, and used C12A7–O^-/27.3%K) were measured by X-ray diffraction (XRD) to investigate the structure characteristic of the catalysts and their changes induced by the ethanol steam reforming process. Figure 8a shows the XRD spectrum for the C12A7–O^- sample, in which the peaks marked by "#" have been assigned to the lattice framework of C12A7–O^- by comparing the peak positions and intensities of the XRD pattern with the data in the Joint Committee of Powder Diffraction Standards (JCPDS) cards. Figure 8b presents the XRD spectrum for the fresh K-doped C12A7–O^- sample (i.e. C12A7–O^-/27.3%K). It was found that the intensities of the peaks corresponding to the C12A7–O^- structure decreased as comparing with those of the C12A7–O^- sample, and this were attributed to the concentration decrease of C12A7–O^- in the C12A7–O^-/27.3%K. However, it is noticed that the C12A7–O^- sample after doping potassium does not destroy the positively charged lattice framework structure of C12A7–O^-. Besides the peaks corresponding to the C12A7–O^- structure, two reproducible peaks at 31.4 ° and 32.6 °, appeared for the C12A7–O^-/27.3%K sample (marked by "*"). By comparing with the crystal phase positions of K_2CO_3, these new peaks were attributed to K_2CO_3. Figure 8c shows the XRD spectrum for the used C12A7–O^-/27.3%K sample by running the steam reforming of ethanol for 4 h (the reaction condition: T = 973 K, S/C = 1.5, GHSV = 10,000 h^{-1}). There are nearly no differences between the diffraction spectrum of the initial C12A7–O^-/27.3%K sample and the used one, and this indicated that the reforming reactions does not destroy the C12A7–O^-/27.3%K structure.

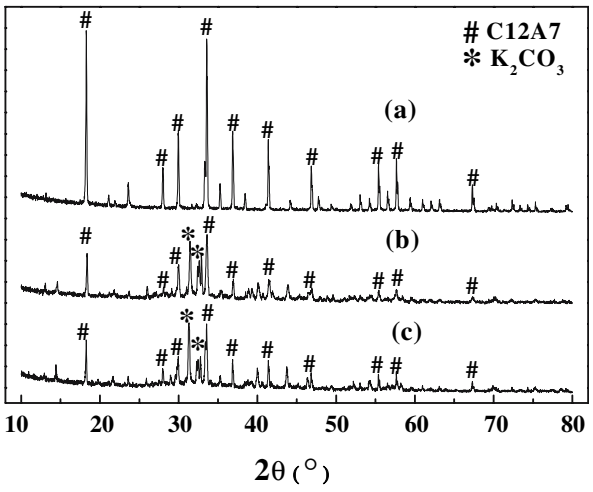

Fig. 8 XRD patterns of (**a**) the fresh C12A7–O^- sample, (**b**) the fresh C12A7–O^-/27.3%K sample, (**c**) the used C12A7–O^-/27.3%K sample after running the steam reforming of ethanol for 4 h (GHSV = 10,000 h^{-1}, S/C = 1.5, T = 973K). By comparing the peak positions and intensities with the data in JCPDS cards, the peaks marked with "#" have been assigned to the structure of C12A7 and those with "*" have been assigned to the structure of K_2CO_3

To further investigate the intermediate species on the C12A7–O^-/27.3%K surface formed during the process of the steam reforming of ethanol, the Fourier Transform Infrared (FT–IR) measurements were employed for the fresh C12A7–O^-/27.3%K and the used one after the steam reforming of ethanol for 4 h (the reforming condition: T = 973 K, S/C = 1.5, GHSV = 10,000 h^{-1}). The absorption envelops in the 450–880 cm^{-1} region are attributed to the C12A7 characteristic absorption structures, corresponding to the Al–O stretching and bending modes in AlO_4 tetrahedral [46]. The two peaks near 1450 and 1377 cm^{-1} are attributed to the K_2CO_3 absorption structures, corresponding to the C–O stretching and bending modes in CO_3^{2-} [47, 48]. Even overlapping with a strong absorption profile around 3400 cm^{-1} (due to the water absorption band of the KBr transparent disk), there is a distinguishable and repeatable peak near 3592 cm^{-1} for the used C12A7–O^-/27.3%K sample after the reforming of ethanol (Fig. 9b). Because the 3592 cm^{-1} band is close to the ν(O–H^-) [28, 49, 50], it was assigned to the stretching vibration of O–H^- on the sample surface. We have confirmed that the O^- anion radicals existed on the surfaces of C12A7–O^- and K-doped C12A7–O^- [18, 19], and it is well known that active O^- anion have strong oxidation power, particularly in the oxidation of hydrocarbons [27–29, 36–38]. Thus it may indicate that the observed OH^- species on the surface were formed by the reactions of ethanol or other hydrocarbons with the active O^- on the C12A7–O^-/27.3%K surface during the ethanol steam reforming.

Futhermore, XPS were employed to investigate the atomic states and the elemental composition both on the

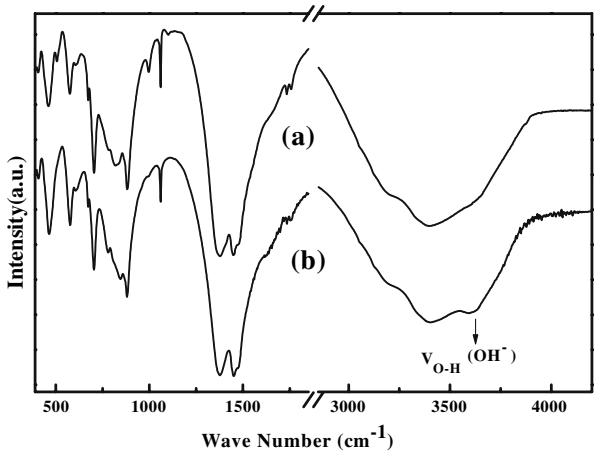

Fig. 9 FT–IR spectra of (**a**) the fresh C12A7–O^-/27.3%K sample, and (**b**) the used C12A7–O^-/27.3%K sample after running the steam reforming of ethanol for 4 h (GHSV = 10,000 h^{-1}, S/C = 1.5, T = 973 K)

fresh C12A7–O^-/27.3%K surface and the used C12A7–O^-/27.3%K surface after the steam reforming of ethanol. Figure 10a shows the XPS spectrum for the C12A7–O^- sample, in which the peaks at 73.3, 346.4, 438.0 and 530.6 eV, have been assigned to Al(2p), Ca($2p_{3/2}$), Ca(2s), O(1s) by comparing the peak positions with the data in the NIST (National Institute of Standards and Technology) Databases. The C(1s) peak at 284.6 eV was used as a calibration standard for determining the peaks' position and the elemental concentration. As shown in Fig. 10b, there were two new peaks appeared at 292.2 and 376.1 ev for the potassium-doped samples of C12A7–O^-/27.3%K that were respectively attributed to K($2p_{3/2}$) and K(2s). The

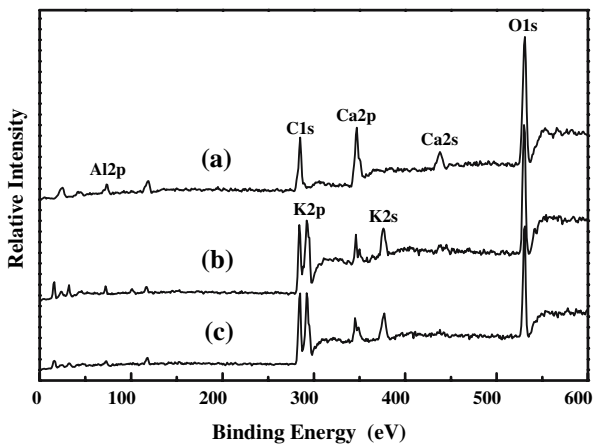

Fig. 10 XPS of (**a**) the fresh C12A7–O^- sample, (**b**) the fresh C12A7–O^-/27.3%K sample, (**c**) the used C12A7–O^-/27.3%K sample after running the reforming of the ethanol for 4 h (GHSV = 10,000 h^{-1}, S/C = 1.5, T = 973K)

K($2p_{3/2}$) and K(2s) peaks were also observed for the the used C12A7–O^-/27.3%K surface after the steam reforming of ethanol (Fig. 10c).

Table 3 shows the atomic concentration of the surface and the bulk of C12A7–O^-/27.3%K, which were estimated by the XPS and ICP-AES measurements, respectively. No significant influence on the potassium concentration by the steam reforming of ethanol was observed under our tested experimental conditions. Moreover, the carbon deposition on the surface of C12A7–O^-/27.3%K was negligible according to the XPS measurements. The binding energy of O(1s) and K($2p_{3/2}$) for three different samples (i.e., C12A7–O^-, fresh C12A7–O^-/27.3%K and used C12A7–O^-/27.3%K after running the ethanol steam reforming for 4 h under GHSV = 10,000 h^{-1}, S/C = 1.5, and T = 973 K) are also given in Table 3. Comparing with the initial C12A7–O^-, the peak position of O(1s) for the fresh C12A7–O^-/27.3%K is slightly shifted from 530.6 eV to the low binding energy of 530.5 eV, which may be caused by the synergetic interaction between C12A7–O^- and the doped potassium. After the ethanol steam reforming reactions, both the peak position of O(1s) and K($2p_{3/2}$) are not significantly changed. The above XPS results show that the steam reforming reactions of ethanol have negligible influences on C12A7–O^-/27.3%K, which agree with the life-time measurement.

Present results shows that the C12A7–O^-/27.3%K catalyst has high activity and selectivity toward hydrogen by the steam reforming of ethanol. For the C12A7–O^-/27.3%K catalyst, 4.73 mol · $mol^{-1}$of the hydrogen yield and 100% of the ethanol conversion was obtained at a molar steam-to-carbon ratio (S/C = 12) and a total gas hourly space velocity (GHSV = 10,000 h^{-1}) at 973 K under atmospheric pressure. The advantages of the C12A7–O^-/*x*%K catalyst may be cheap, environmentally friendly, and possessing a long-term stability. Particularly, negligible carbon deposition was formed even for S/C ratio equal to the stoichiometric one, which would be more appropriate to the hydrogen production from ethanol steam reforming. It was noticed that the active O^- appeared both in the bulk and on the surface of C12A7–O^- or K-doped samples [18–20] and have a high reactivity, particularly in strong oxidation for hydrocarbons [27–29, 36–38]. The active species of O^- may be involved in the steam reforming of ethanol, because the intermediate of OH^- has been observed by FT–IR. Moreover, the addition of potassium to C12A7–O^- would play a cooperative role in the steam reforming of ethanol over the C12A7–O^-/*x*%K catalyst. It was also found that adding potassium significantly enhanced the hydrogen yield as well as the ethanol conversion, and decreased the carbon-deposited on the catalyst due to the increased rate of carbon gasification [43].

Table 3 The surface atomic concentration, the bulk atomic concentration, and the binding energy for the fresh C12A7–O^- sample, the fresh C12A7–O^-/27.3%K sample, and the used C12A7–O^-/27.3%K sample after running the steam reforming of the ethanol for 4 h (GHSV = 10,000 h^{-1}, S/C = 1.5, T = 973K)

samples	$K_{surface}$ (mol%)[a]	K_{bulk} (wt%)[b]	$C_{surface}$ (mol%)[c]	O1s (eV)	$K2p_{3/2}$ (eV)
C12A7–O^-	0	0	0	530.6	–
Fresh C12A7–O^-/27.3%K	21.5	27.3	0	530.5	292.2
Used C12A7–O^-/27.3%K	21.7	27.2	0.02	530.5	292.2

[a] The K molar concentration on the sample surface measured by XPS

[b] The K weight percent in the samples measured by ICP-AES

[c] The C molar concentration on the sample surface measured by XPS. The amount of carbon adding for the calibration has been deducted

4 Conclusions

The present investigation shows that the C12A7–O^-/27.3%K catalyst exhibits high catalytic activity and long stability for the reaction of ethanol steam reforming. The catalyst is very selective to hydrogen production, depending on the experimental conditions. Both the hydrogen yield and the carbon conversion over the C12A7–O^-/27.3%K catalyst were sensitive to temperature, the S/C ratio, the contact time and the potassium-doped content in the catalysts. Carbon formation was found to be negligible even for the molar ratio of H_2O/C_2H_5OH equal to the stoichiometric one. The advantages of the C12A7–O^-/*x*%K catalyst would be cheap and environmentally friendly, and possessing a long-term stability, which would be useful to the hydrogen production from ethanol steam reforming. Based on the characterization, it was found that the active oxygen species and the doped potassium play important roles in the steam reforming of ethanol over the C12A7–O^-/*x*%K catalyst.

Acknowledgments The authors are grateful to the support of "863 Program" of Ministry of Science and Technology of China (No. 2006AA05Z118) and "BRP program 2002" of Chinese Academy of Sciences.

References

1. Armor JN (1999) Appl Catal A 176:159
2. Song C (2002) Catal Today 77:17
3. Das D, Veziroglu TN (2001) Int J Hydrogen Energy 26:13
4. Llorca J, Homs N, Sales J, Pilar R de la Piscina (2002) J Catal 209:306
5. Freni S, Cavallaro S, Mondello N, Spadaro L, Frusteri F (2003) Catal Commun 4:259
6. Liguras K, Kondarides DI, Verykios XE (2003) Appl Catal B 43:345
7. Aupretre F, Descorme C, Duprez D (2002) Catal Commun 3:263
8. Roh HS, Wang Y, King DL, Platon A, Chin YH (2006) Catal Lett 108:15
9. Kugai J, Velu S, Song C (2005) Catal Lett 101:255
10. Fatsikostas AN, Kondarides DI, Verykios XE (2002) Catal Today 75:145
11. Klouz V, Fierro V, Denton P, Katz H, Lisse JP, Bouvot-Mauduit S, Mirodatos C (2002) J Power Sources 105:26
12. Marino F, Boveri M, Baronetti G, Laborde M (2004) Int J Hydrogen Energy 29:67
13. Hosono H, Abe Y (1987). Inorg Chem 26:1192
14. Hayashi K, Matsuishi S, Kamiya T, Hirano M, Hosono H (2004) Nature 419:462
15. Hayashi K, Matsuishi S, Ueda N, Hirano M, Hosono H (2003). Chem Mater 15:1851
16. Yang S, Konda JN, Hayashi K, Hirano M, Domen K, Hosono H (2004) Chem Mater 16:104
17. Matsuishi S, Toda Y, Miyakawa M, Hayashi K, Kamiya T, Hirano M, Tanaka I, Hosono H (2003) Science 301:626
18. Hayashi K, Hirano M, Matsuishi S, Hosono H (2002) J Am Chem Soc 124:738
19. Li QX, Hosono H, Hirano M, Hayashi K, Nishioka M, Kashiwagi H, Torimoto Y, Sadakata M (2003) Surf Sci 527:100
20. Li QX, Hayashi K, Nishioka M, Kashiwagi H, Hirano M, Hosono H, Sadakata M (2002). Appl Phys Lett 80:4259
21. Li QX, Hayashi K, Nishioka M, Kashiwagi H, Hirano M, Torimoto Y, Hosono H, Sadakata M (2002) Jpn J Appl Phys 41:L530
22. Huang F, Li J, Xian H, Tu J, Sun JQ, Yu SQ, Torimoto Y, Sadakata M, Li QX (2005) Appl Phys Lett 86:114101–1
23. Li J, Huang F, Wang L, Yu SQ, Torimoto Y, Sadakata M, Li QX (2005) Chem Mater 17:2771
24. Deubel DV, Frenking G (1999) J Am Chem Soc 121:2021
25. Fessenden RW, Meisel D (2000) J Am Chem Soc 122:3773
26. Lee J, Grabowski JJ (1992) Chem Rev 92:1611
27. Born M, Ingemann S, Nibbering NMM (1997) Mass Spectrometry Rev 16:181
28. Tashiro T, Watanabe T, Kawasaki M, Toi K (1993) J Chem Soc Faraday Trans 89:1263
29. (a) Aika KI, Lunsford JH (1977) J Phys Chem 81:1393; (b) Ito T, Tashiro T, Kawasaki M, Watanabe T, Toi K (1991) J Phys Chem 95:4476
30. Neophytides SG, Tsiplakides D, Stonehart P, Jaksic MM, Vayenas CG (1994) Nature 370:45
31. Lemonidou AA, Vasalos IA (1989) Appl Catal 54:119
32. Kumar VA, Pant KK, Kunzru D (1997) Appl Catal A 162:193
33. Pant KK, Kunzru D (1994) Ind Eng Chem Res 36:2059
34. Pant KK, Kunzru D (2002) Chem Eng J 87:219
35. Pant KK, Kunzru D (1998) Chem Eng J 70:47
36. Goula MA, Lemonidou AA, Grunert W, Baerns M (1996) Catal Today 32:149
37. Yang S, Kondo JN, Hayashi K, Hirano M, Domen K, Hosono H (2004) Appl Catal A 277:239
38. Dong T, Li J, Huang F, Wang L, Tu J, Torimoto Y, Sadakata M, Li QX (2005) Chem Comm 21:2724
39. Xian H, Pan Y, Qiu SB, Tu J, Zhu XF, Li QX (2005) Chin J Chem Phys 18:469
40. Wen WY (1980) Catal Rev Sci Eng 22:1
41. Wood BJ, Sapcier KM (1984) Catal Rev Sci Eng 26:233
42. Hüttinger KJ, Minges R (1986) Fuel 65:1112

43. Mukhopadhyay R, Kunzru D (1993) Ind Eng Chem Res 32:1914
44. Nowak S, Zimmermann G, Guschel H, Anders K (1990) Catalysis in petroleum refining 1989, Elsevier Amsterdam, p 103
45. Fatsikostas AN, Verykios XE (2004) J Catal 225:439
46. Schroeder RA, Lyons LL (1966) J Inorg Nucl Chem 28:1155
47. Černák J, Ferencová B, Žák Z (2005) Polyhedron 24:579
48. Huang W, Sun PY, Fang JL, Sun YF, Gou SH (2003) Trans Metal Chem 28:925
49. Datta RK (1987) J Am Ceram Soc 70:C288
50. Henderson B, Sibley WA (1971) J Chem Phys 55:1276
51. Jeevaratnam J, Glasser FP, Glasser LSD (1964) J Am Ceram Soc 47:105